

Synthesis and Study of Superhigh-Concentrated Organosols of Silver Nanoparticles

S. A. Vorobyev^{a, *}, M. Yu. Flerko^a, S. A. Novikova^a, E. V. Mazurova^a, Ye. V. Tomashevich^a, M. N. Likhatski^a, S. V. Saikova^{a, b}, A. S. Samoilo^b, N. A. Zolotovskiy^c, and M. N. Volochaev^{c, d}

^a Institute of Chemistry and Chemical Technology, Siberian Branch, Russian Academy of Sciences, Krasnoyarsk, 660036 Russia

^b Siberian Federal University, Krasnoyarsk, 660041 Russia

^c Kirenskii Institute of Physics, Siberian Branch, Russian Academy of Sciences, Krasnoyarsk, 660036 Russia

^d Tomsk National Research State University, Tomsk, 634050 Russia

*e-mail: yekspatz@ya.ru

Received November 3, 2023; revised December 6, 2023; accepted December 6, 2023

Abstract—Due to their unique properties, organosols of silver nanoparticles are widely used in optical and semiconductor devices, to produce electrically and thermally conductive films, as catalysts, antibacterial materials, etc. This work proposes a simple and highly productive method for the preparation of silver organosols, which have a metal concentration as high as 1800 g/L and contain spherical nanoparticles with low polydispersity and a median size of 9.1 nm. The method consists in the initial preparation of silver nanoparticle hydrosols with a concentration of higher than 30 g/L followed by the transfer of the NPs into an organic phase of *o*-xylene. A set of physical research methods has been employed to study the regularities of the extraction of silver nanoparticles with *o*-xylene in the presence of cetyltrimethylammonium bromide (CTAB) and ethanol and to determine the optimal process conditions, under which the extraction degree is as high as 62.5%. It has been found that bromine anions contained in CTAB molecules cause the aggregation of some amount of silver nanoparticles with the formation of silver metal sediment in the aqueous phase. According to X-ray photoelectron spectroscopy data, the sediment contains bromide ions (up to 4 at %) on the particle surface. Organosols synthesized under optimal conditions are stable for more than 7 months and withstand repeated cycles of drying and redispersing. Silver organosols have been used to obtain metal films with an electrical conductivity of about 68 500 S/cm, which increases to 412 000 and 509 500 S/cm (87.8% of the electrical conductivity of bulk silver) after thermal treatment at 150 and 250°C, respectively.

Keywords: silver nanoparticles (NPs), concentrated silver organosols, phase transfer of nanoparticles, X-ray photoelectron spectroscopy (XPS), transmission electron microscopy (TEM), conductive silver films

DOI: 10.1134/S1061933X23601294

INTRODUCTION

Organosols of silver nanoparticles can be used for the production of optical devices, chemical and biological sensors, catalysts, antibacterial materials, inks for 2D and 3D printing, composite materials, etc. [1–7].

Among numerous methods employed to produce silver organosols, the phase transfer method has gained the greatest popularity. This method consists in the initial preparation of hydrosols of silver nanoparticles followed by transfer of particles into an organic phase using surfactants and so-called “phase-transfer catalysts” [8–15]. Hydrosols are obtained by reducing aqueous AgNO₃ solutions with NaBH₄ [8, 9], formamide [11], hydrazine [12], and other reductants. Toluene [10], CHCl₃ [11], cyclohexane [12], hexadecylamine [13], methanol [14, 15], etc., are used as organic solvents. Formamide, oleic acid, cetyltrimethylammonium bromide (CTAB), NaCl, thiols, hexylamine,

dodecylamine, etc., are used to stabilize obtained hydrosols and increase transfer efficiency [8–15].

This approach makes it possible to easily control the sizes and morphology of nanoparticles, as well as to relatively easily isolate them and purify from impurities by selective transfer into an organic phase. However, in most procedures presented in the literature and patents, the concentration of silver nanoparticles in initial hydrosols and organosols obtained from them seldom exceeds 0.5–1 g/L. The use of such low-productive synthesis methods leads to a decrease in the efficiency and profitability of their production and causes the need in the disposal and recycling of large amounts of waste solutions.

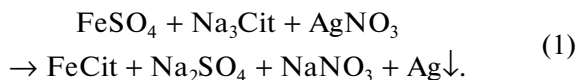
Previously, we used the citrate–sulfate procedure (the so-called Carey Lea method [16]) to develop a simple and highly productive technology for the synthesis of uniform high-concentrated silver dispersions, which had metal concentration of 30–2100 g/L

and were stable with respect to aggregation [17–20]. The goal of this work was to study the features of the transfer of Ag⁰ NPs from an aqueous phase into *o*-xylene in the presence of cetyltrimethylammonium bromide, as well as to reveal the regularities of changes in the physicochemical properties of silver nanoparticles upon the passage from hydrosols to materials based thereon.

EXPERIMENTAL

The following reagents were used in the work: AgNO₃, Na₃Cit·5.5H₂O, and FeSO₄·7H₂O (Khimreaktivsnab); *o*-xylene (EKOS-1); CTAB (Fluka); and ethanol (95%, Constanta-Pharm M). All reagents were of the reagent or extra pure grade and used as received. Aqueous solutions of the reagents were prepared immediately before experiments in deionized water of the Milli-Q grade.

Silver metal nanoparticles were synthesized at room temperature under stirring on a magnetic stirrer at 200 rpm. An AgNO₃ solution (50 mL, 0.6 M) was added to a mixture of aqueous solutions of FeSO₄ (50 mL, 1.08 M) and sodium citrate (70 mL, 1.36 M); then, the reaction mixture was stirred for 5 min more. The following reaction yielded a black–brown sediment of coagulated silver nanoparticles:



To purify the particles from soluble reaction products and intact reagents, the coagulant was centrifuged for 5 min at 1000 rpm, the sediment was separated and peptized in water (25 mL); the nanoparticles were coagulated once more under the action of a sodium citrate solution (25 mL, 0.3 M), and centrifuged again. The coagulation–centrifugation–peptization procedure was repeated 3–4 times; thereafter, the sediment was peptized in the initial volume of deionized water. The hydrosols purified in this way contained less than 3 wt % sodium citrate and trace amounts of iron ions.

To extract nanoparticles into the organic phase, deionized water and other reagents were added to purified silver hydrosol (20 mL) to reach the following final concentrations: silver, 0.2–0.6 M; ethanol, 0–6 M; and CTAB, 2.5–20.0 mM. Then, *o*-xylene (5–40 mL) was added; the mixture was stirred gently for 15 min and centrifuged for 5 minutes at 2000 rpm. After centrifugation, the mixture separated into a dark-yellow upper organic layer and a colorless aqueous layer with some amount of black sediment at the bottom. The organic phase was decanted. The solvent was removed under reduced pressure at 30°C until the metal concentration in the organosol reached 1800 g/L or the sample was completely dry. The sediment was thoroughly washed with deionized water and dried at room temperature in air in the dark.

To determine the concentration of silver in hydro- and organosols, a colloidal solution (1 mL) was exposed at 150°C until the solvent was completely removed, the beaker was cooled to room temperature, and concentrated nitric acid (2 mL) was added to dissolve silver. The solution was re-evaporated at 150°C until white AgNO₃ crystals arose. The beaker was cooled to room temperature, AgNO₃ crystals were dissolved in water, Fe(NO₃)₃ was added, and titration was performed with 0.1 M KSCN standard titer under stirring until a stable pink color arose. The results obtained were used to calculate the extraction degree as the ratio of the number of moles of silver that passed into the organic phase to the initial number of moles of silver in the hydrosol.

Analysis of the stability of organosols with respect to repeated drying–peptization cycles was carried out by completely removing the solvent from an organosol (1 mL) in vacuum and treating the resulting sediment with *o*-xylene (1 mL). After four cycles, a sample (5 μL) of organosol was taken and diluted with *o*-xylene (20 mL); then, electronic absorption spectra (EAS) were recorded.

To obtain conductive films, a concentrated silver organosol (20 μL) was applied onto a dry degreased cover glass 24 × 24 mm² in size (OOO MiniLab) using the Doctor Blade Coating method [21] and dried in air. The glass plates were prepared by treating alternately with 2M NaOH, alcohol, and acetone in an ultrasonic bath for 10 min and rinsing thoroughly with deionized water after each step; then, the plates were air dried. The resulting films had a typical silvery color and a rather high electrical conductivity. The films were annealed at temperatures of 100–250°C for 2 h in air in an LF-15/13-V2 programmable laboratory oven (LOIP, Russia). The samples were heated in the oven at a rate of 10°C/min to a preset temperature and incubated for 2 h. Then, the oven was turned off, while the samples were kept in it for 5–12 h until they were cooled to 40–60°C; thereafter, the samples were withdrawn. Before and after annealing, the electrical conductivity of the films was measured by the four-probe method using an ST-2258C multimeter (JG, China). At least 20 measurements were carried out; the error did not exceed 2%. The average film thicknesses were estimated by performing 5–10 scanning electron microscopic (SEM) measurements of cleavages obtained from different regions.

X-ray photoelectron spectra (XPS) were recorded using a SPECS spectrometer (SPECS, Germany) equipped with a PHOIBOS150 MCD-9 analyzer. Monochromatic AlK_α radiation (1486.6 eV) was employed. The pressure in the analytical chamber was 10^{−9} mbar. Dynamic light scattering (DLS) studies of nanoparticle sols were carried out in a glass cell at a temperature of 25°C using a Zetasizer Nano ZS spectrometer (Malvern, United Kingdom) operating at a scattering angle of 173°. Optical absorption spectra

were recorded within a wavelength range of 190–760 nm in quartz cells with a light path of 1 cm using an AvaSpec2048L instrument (Avantes, the Netherlands). Micrographs of nanoparticles were obtained with an HT7700 transmission electron microscope (TEM) (Hitachi, Japan) operating at an accelerating voltage of 80 kV. TEM particle size distribution statistics was estimated on the basis of 3032 and 991 micrographs for the initial hydrosol and organosol, respectively. SEM examinations were carried out with an SU3500 instrument (Hitachi, Japan) operating at an accelerating voltage of 20 kV. X-ray diffraction (XRD) analysis of dried samples was carried out with a Shimadzu XRD-6000 device (Shimadzu Corporation, Japan) using monochromatic $\text{CuK}\alpha$ radiation. Phase identification was carried out with the help of the PDF₄ database file. Cell parameters were refined and coherent-scattering region (CSR) sizes were determined using the Topas₃ software by the Rietveld method. FTIR spectra were recorded using pellets containing KBr (1 g) and a dried sample (2 mg) with a Vector 22 FTIR spectrometer (Bruker, Germany). Thermogravimetric measurements (TG/DTG) and differential scanning calorimetry (DSC) were carried out using an SDT Q600 synchronous thermal analyzer equipped with a Nicolet 380 FTIR attachment for exhaust gas analysis within a temperature range of 25–1000°C at a heating rate of 20°C/min and a gas flow rate of 50 mL/min in an oxidative atmosphere (N_2 , 80 vol %; O_2 , 20 vol %).

RESULTS AND DISCUSSION

*Determination of Optimal Conditions for the Extraction of Silver Nanoparticles with *o*-Xylene*

In preliminary studies of the extraction of silver nanoparticles with *o*-xylene from an aqueous phase, diverse additives of organic compounds were studied: dodecanethiol, sodium dodecyl sulfate, allylamine, octylamine, decylmethylamine, dioctylamine, etc. However, a satisfactory result was obtained only when using a cationic surfactant, cetyltrimethylammonium bromide (CTAB).

n-Alkanes, such as C_6H_{14} , C_7H_{16} , C_8H_{18} , C_9H_{20} , $\text{C}_{10}\text{H}_{22}$, and $\text{C}_{12}\text{H}_{24}$, were also tested as organic media for extraction; however, the extraction efficiency was less than 10%, other conditions being equal. The use of carcinogenic benzene and toluene was not considered. Being slightly volatile, moderately toxic, and relatively cheap (~500 rubles/L), *o*-xylene appeared to be most efficient in the extraction process.

Initial silver hydrosols with a concentration of 30 g/L had a pH value of 8.3 and a zeta potential of –35 mV [20]. The negative surface charge of silver nanoparticles was likely due to the specific adsorption of citrate anions. In this case, according to the XPS data (Table 1), the charge is compensated by sodium cations present in the electrical double layer (EDL).

Table 1. Atomic concentrations (%) of elements on the surface of silver nanoparticles: initial particles, particles after extraction, and unextractable with *o*-xylene

Sample	Ag	O	C	Br	N	Na
Hydrosol	13.0	29.4	51.5	–	–	6.1
Organosol	5.7	6.2	86.3	–	1.8	–
Sediment	19.0	6.0	71.3	3.7	–	–

Upon treatment with cetyltrimethylammonium bromide, these cations are replaced by $\text{C}_{16}\text{H}_{33}\text{N}(\text{CH}_3)_3^+$ cations (in the organosols, nitrogen atoms are present and sodium atoms are absent on the surface of silver NPs, Table 1). This probably increases the hydrophobicity of the surface of silver nanoparticles, thereby promoting their transition into the phase of *o*-xylene (Fig. 1a).

However, as the amount of CTAB was further increased, the degree of silver extraction dramatically decreased at all its studied concentrations, and a black sediment arose in a hydrosol.

The extraction degree of nanoparticles (Fig. 1b) increased almost linearly with increasing ethanol concentration from 0 to 6 M. Probably, ethanol molecules acted as “phase-transfer catalysts” reducing the surface tension at the *o*-xylene–water interface and facilitating the transition of nanoparticles into the organic phase [15].

Dependences of the extraction degree on CTAB concentration at different $V_{\text{xylene}} : V_{\text{sol}}$ volume ratios in a range of 0.5–2 (not shown) were close to each other and similar to the curves presented in Fig. 1b. However, with a decrease in the $V_{\text{xylene}} : V_{\text{sol}}$ ratio to 0.25, the extraction degree drastically decreased. The maximum degree of NP extraction (62.5%) was observed at $V_{\text{xylene}} : V_{\text{sol}} = 2$, silver NP concentration in the initial hydrosol of 0.4 M, CTAB concentration of 10 mM, and ethanol concentration of 2 M.

Figure 2 (curves 1) presents the electronic absorption spectra of the initial silver hydrosol. The spectra contain a surface plasmon resonance (SPR) band with a maximum at 393 nm characteristic of Ag^0 nanoparticles [17, 18]. However, after metal extraction with *o*-xylene (curves 2) the intensity of the SPR maximum decreased due to a reduction in the concentration of Ag NPs in the organic phase as compared with their concentration in the hydrosol. Moreover, the maximum shifted to 416–423 nm and a shoulder arose in a range of 510–540 nm probably because of particle aggregation. The bathochromic shift of the SPR maximum was caused by a change in the optical properties of the particles as a result of the adsorption of cetyltrimethylammonium cations rather than by an increase in the particle sizes, as was confirmed by the TEM data [13].

Organosols obtained under optimal conditions ($C_{\text{Ag}} = 0.4 \text{ M}$, $C_{\text{CTAB}} = 10 \text{ mM}$, $V_{\text{xylene}} : V_{\text{sol}} \geq 0.5$,

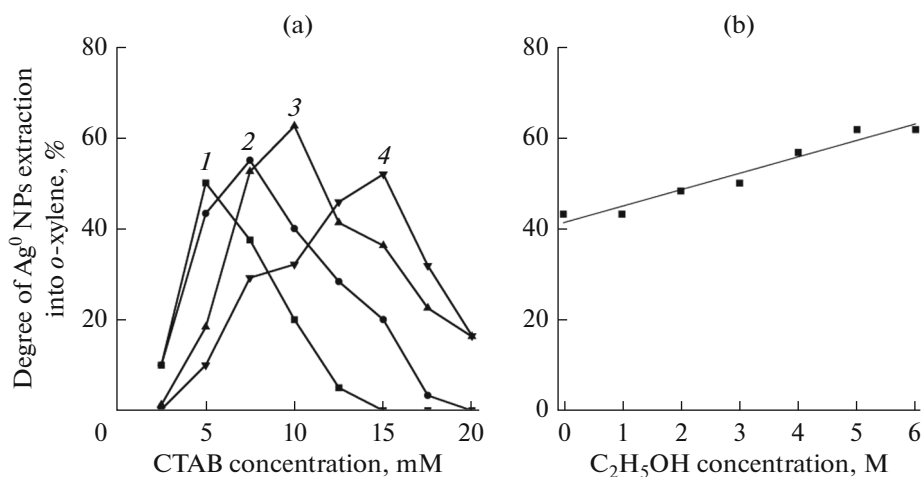


Fig. 1. The influence of (a) CTAB and (b) ethanol concentrations on the degree of silver extraction at different initial Ag⁰ concentrations: (1) 0.2, (2) 0.3, (3) 0.4, and (4) 0.5 M. [(a) ($C_{C_2H_5OH} = 2$ M, $V_{xylene} : V_{sol} = 2$); (b) ($C_{Ag} = 0.4$ M, $C_{CTAB} = 15$ mM, $V_{xylene} : V_{sol} = 2$)].

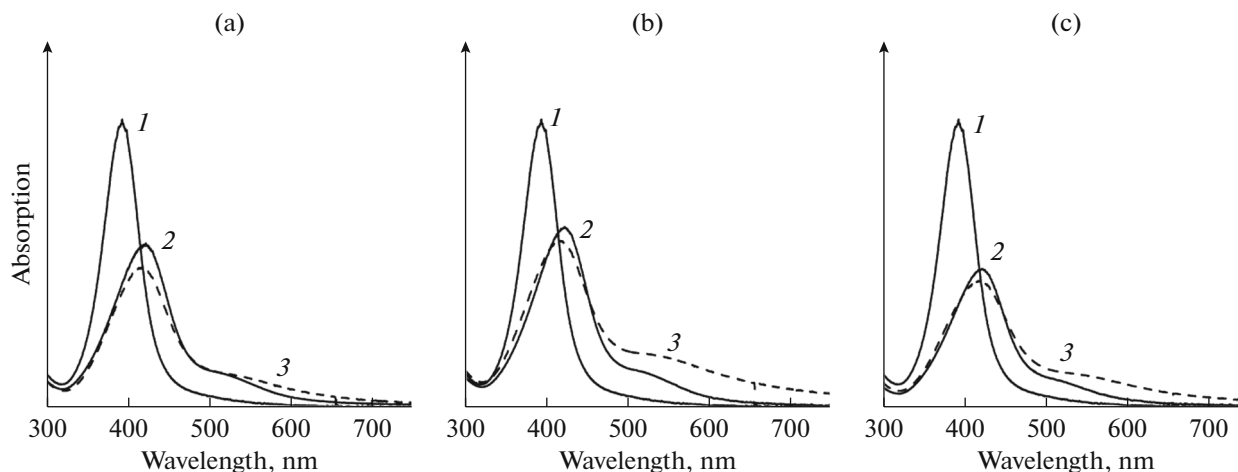


Fig. 2. Optical absorption spectra of (1) initial hydrosol, (2) freshly obtained organosol, and (3) organosol after four successive cycles of drying and peptization. $C(CTAB)$ (mM): (a) 7.5, (b) 10, and (c) 12.5.

$C_{C_2H_5OH} = 2$ M) withstood several cycles of drying in vacuum at room temperature and redispersing in *o*-xylene. Moreover, after four drying–redispersing cycles, there was only a slight broadening of the SPR maximum and an increase in the intensity of the shoulder at 510–540 associated with a slight increase in the fraction of aggregated NPs (Fig. 2, curves 3). The high stability of the obtained organosols made it possible to increase the metal concentration in them to 1800 g/L by partial removal of the solvent, while the sols retained their stability for more than 7 months.

Study of Hydro- and Organosols of Silver

According to TEM data (Fig. 3), the initial silver hydrosols contained almost spherical nanoparticles

with a median size of 8.4 nm. After the extraction into the phase of *o*-xylene, the shape of the particles remained actually unchanged. As in the hydrosol, the particle size distribution in the organosol was lognormal, thereby indicating the presence of some amount of aggregates. The median particle size after the transition to the organic phase slightly increased to 9.1 nm.

X-ray phase analysis (Fig. 4a) of all obtained samples confirmed the presence of only one phase of silver metal (JCPDS, 4-0783) in them. Refinement of diffraction patterns using the Rietveld method showed that the CSR for the initial nanoparticles was 7.7 ± 0.1 nm; after their extraction with *o*-xylene, it increased to 11.7 ± 0.1 nm, thus being in good agreement with the TEM data. The sediment formed in the aqueous phase during extraction was also the phase of pure silver

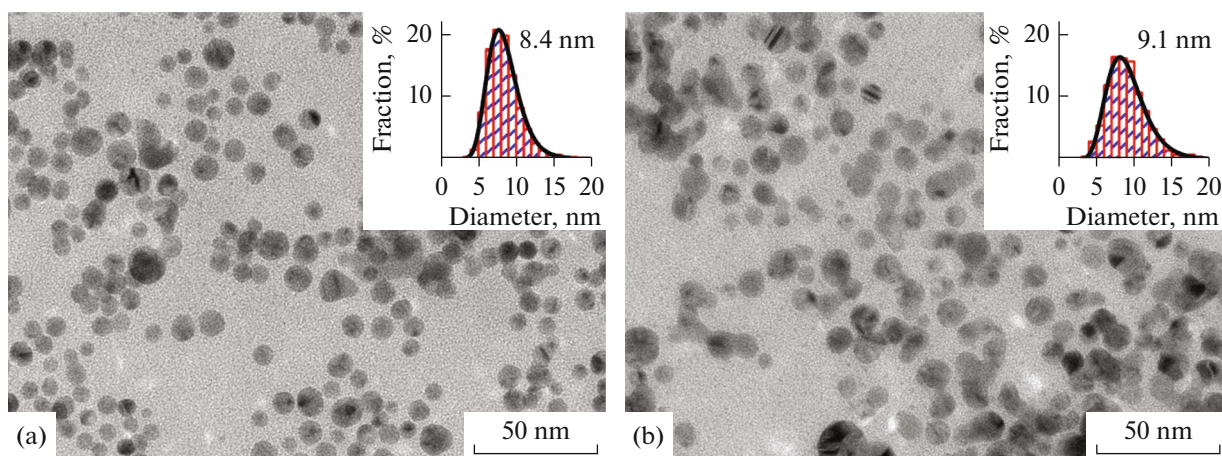


Fig. 3. TEM microphotographs and corresponding histograms of nanoparticle size distribution in (a) initial hydrosol and (b) after extraction of nanoparticles with *o*-xylene.

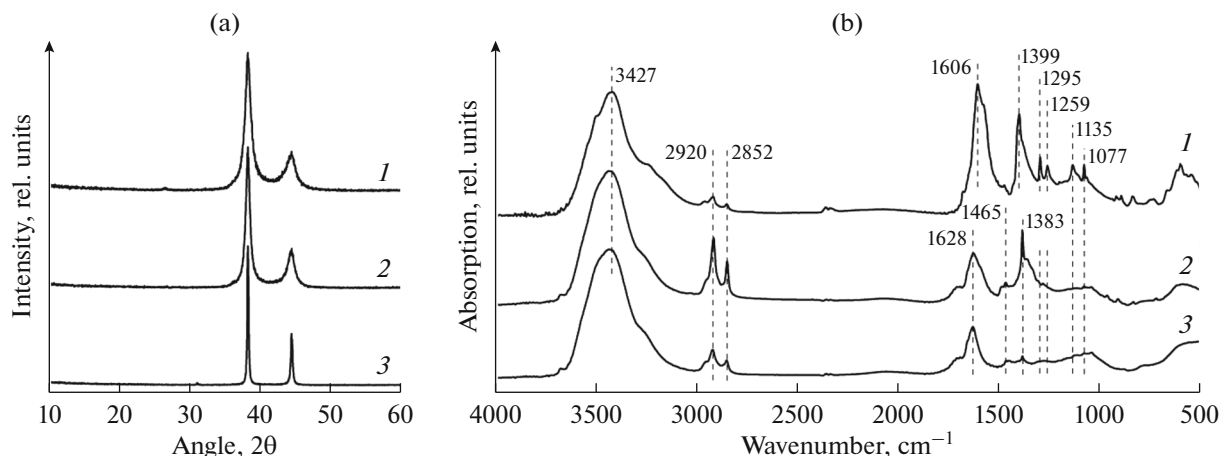


Fig. 4. (a) X-ray phase analysis and (b) FTIR spectra of dried samples of (1) initial silver hydrosols, (2) silver organosols, and (3) sediment unextractable with *o*-xylene.

metal; however, the CSR in this sample was 71.3 ± 0.8 nm, probably, due to the Ostwald ripening processes [23].

The IR spectra (Fig. 4b) of the initial silver nanoparticles contain a wide absorption band inherent in the stretching vibrations of adsorbed water and structural OH groups (3427 cm^{-1}), asymmetric and symmetric stretching vibrations of C–H bonds (2920 and 2852 cm^{-1}), asymmetric vibration of C–OH bonds (1295 and 1077 cm^{-1}), C–O stretching (1135 cm^{-1}) and C–O stretching vibrations (1259 cm^{-1}), and symmetric and asymmetric vibrations of COO^- (1606 and 1399 cm^{-1}) carboxyl groups [18, 24]. A group of weak bands in the region $980\text{--}820 \text{ cm}^{-1}$ could not be reliably identified. The presence of aliphatic, hydroxyl, and carboxyl groups in the sample confirmed the adsorption of citrate ions on the nanoparticle surface, with this adsorption ensuring

their stability in multiple coagulation–peptization processes.

After treatment with ethanol and CTAB and extraction, there was a natural increase in the intensity of the absorption bands of C–H bond vibrations at 2920 and 2852 cm^{-1} , as well as the appearance of weak bands of bending vibrations for the C–N⁺ bond at 1465 cm^{-1} . In addition, a decrease was observed in the relative intensity of the bands of symmetric and asymmetric stretching of COO^- and their shift to the regions of 1628 cm^{-1} and 1383 cm^{-1} . However, overlap of the 1628 cm^{-1} band with a characteristic absorption band of scissor vibrations of water at 1636 cm^{-1} cannot be ruled out. Apparently, there was a change in the nature and strength of binding of citrate carboxyl groups to the nanoparticle surface and a decrease in their amount upon the treatment with CTAB [18, 24]. In the IR spectra of the sediment, a significant

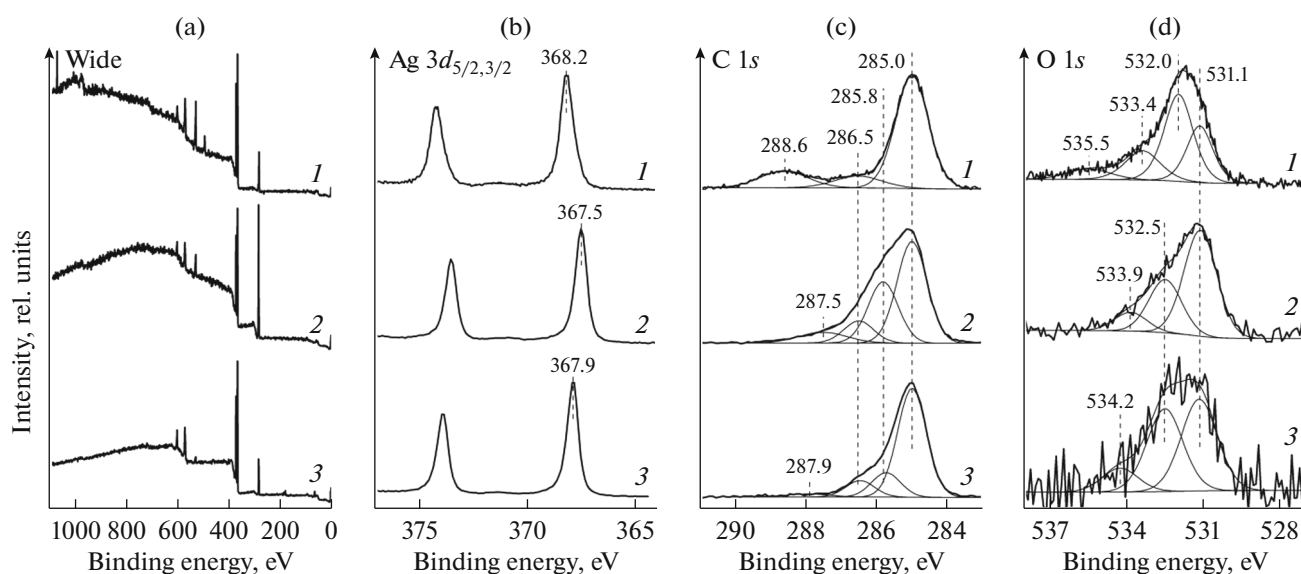


Fig. 5. XPS spectra: (a) survey, (b) Ag $3d$, (c) C $1s$, and (d) O $1s$ of (1) initial silver nanoparticles, (2) organosols, and (3) sediment formed in hydrosol during extraction.

decrease in the intensity of the absorption band for C–H vibrations and the almost complete disappearance of all other bands was observed, except for the absorption band at 1628 cm^{-1} .

The results obtained were confirmed by X-ray photoelectron spectroscopy data. The survey spectra contained lines of Ag, O, C, Br, N, and Na (Table 1, Fig. 5a). As discussed above, the presence of sodium ions on the surface of the initial silver nanoparticles, was associated with the adsorption of sodium citrate.

The surface of Ag^0 NPs in the organic phase contains higher concentrations of carbon and lower concentrations of oxygen than those in the hydrosols, as well as nitrogen atoms due to the adsorption of CTAB. Since there are no bromine lines on the surface of this sample, it is likely that cetyltrimethylammonium cations replace Na^+ in the EDL. The silver sediment formed in the aqueous phase during extraction, on the contrary, contains bromide ions, probably due to their adsorption on the surface of nanoparticles, which leads to their aggregation and sedimentation [22].

Ag $3d_{5/2}$ line (Fig. 5b) in the spectrum of the initial nanoparticles had a binding energy of about 368.2 eV characteristic of silver metal [20]. However, in the organosol, the binding energy shifted to 367.5 eV apparently due to the adsorption of quaternary ammonium cations on the particle surface or silver surface oxidation [25]. In the silver sediment, the binding energy was 367.9 eV, which could correspond to the formation of some amount of AgBr on the surface of the particles [26].

The C $1s$ carbon line (Fig. 5c) in the spectrum of the initial silver nanoparticles contained signals of aliphatic carbon at 285.0 eV (C–H, C–C), alcohol

groups at 286.5 eV (R–OH), and carboxyl groups at 288.6 eV (COO^-) of adsorbed sodium citrate [27–29]. After treatment with CTAB solutions, a component of carbon bound to nitrogen arose in the spectra at 285.8 eV (C– N^+); a decrease in the relative contribution of COO^- and R–OH groups and a reduction in binding energy to 287.5 eV for COO^- were observed. This may also indicate the sorption of cetyltrimethylammonium cations on the surface of nanoparticles.

The O $1s$ line (Fig. 5d) of the initial nanoparticles contained components corresponding to oxygen of OH groups (531.1 eV), $-\text{COO}^-$ groups (532.0 eV), alcohol group R–OH (533.4 eV), and adsorbed water (535.5 eV) [17–20]. After the treatment with CTAB solutions, the binding energy of the groups remaining on the surface increased to 532.6 eV ($-\text{COO}^-$) and 533.9 eV (R–OH) probably due to the transfer of electron density from the sorbed cetyltrimethylammonium cation to the oxygen atom in the $-\text{COO}^-$ group [30].

Study of Films Obtained by Deposition of Silver Organosols

The TG and DSC curves measured for the dried organosol in the air atmosphere are presented in Fig. 6a. In a temperature range of 25–400°C, the TG curve exhibits several stages of mass loss accompanied by weakly expressed exothermic maxima at 207 and 282°C against the strong endothermic background, as well as an exothermic effect at 343°C. At $T < 100^\circ\text{C}$, the solvent was removed. Analysis of the exhaust gases (Fig. 6b) recorded the removal of esters in a range of 180–260°C (maximum at 220°C), mixtures of alkanes and/or ketones in a range of 190–390°C (maximum at

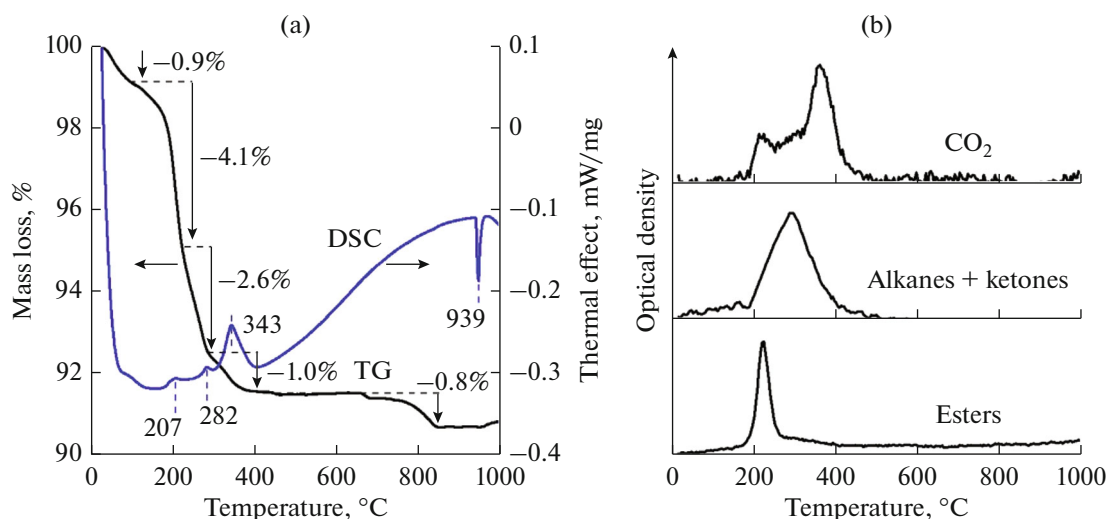


Fig. 6. (a) Results of a thermal studying dried organosols of silver NPs and (b) temperature dependences of IR signal intensities of exhaust gases.

290°C) and carbon dioxide in a range of 180–400°C. These substances are the products of the thermal decomposition and partial oxidation of residual solvent and organic compounds adsorbed on the surface of nanoparticles. A decrease in sample mass by 0.8% in a temperature range of 660–850°C occurred without pronounced thermal effects and was not registered in the IR spectra. A pronounced endothermic effect in the DSC curve at 939°C unaccompanied by a change in mass corresponded to the melting of silver nanoparticles, which, due to size effects, occurred almost 23°C lower than the melting temperature of bulk silver [31].

The obtained silver organosols with a concentration of 800–1000 g/L were applied onto a dry degreased surface of a cover glass using the Doctor Blade Coating method [21]. Evaporation of *o*-xylene at room temperature left a spot with a typical metallic luster and a low electrical resistance (about 68500 S/cm). The resulting films had a good adhesion to the surface and, if necessary, could be washed off with *o*-xylene or hexane. According to the SEM data (Fig. 7), the films had the same thickness (1 μm) and a slight roughness and were formed by submicron-sized agglomerates consisting of smaller particles. It was found that, in one application procedure, as a result of increasing the volume of organosol applied per unit area of the substrate, thicker films (up to 20 μm) could be obtained.

When the obtained films were heated in air (Fig. 8) for 2 h, the surface color changed to matte white and the electrical conductivity increased to 76164 S/cm (25°C) already at 100°C. With a further increase in the annealing temperature to 150°C, the specific electrical conductivity grew by almost six times and reached a value of 411939 S/cm, which amounted to 66.4% of

the electrical conductivity of the bulk silver sample at this temperature.

After annealing the initial films for 2 h at a temperature of 250°C, the film thickness decreased almost twofold due to sintering of the initial nanoparticles with the formation of a pronounced fine structure formed by submicron silver particles with insignificant porosity. In this case, the electrical conductivity of the films reached 509500 S/cm, which corresponded to 87.8% of the electrical conductivity of bulk silver. It is worth noting that, according to literature data, during the heat treatment at 250°C [32] or laser sintering [33] of conductive ink formed by silver nanoparticles, the specific electrical conductivity of the resulting material seldom exceeds 20% of the conductivity of bulk silver.

CONCLUSIONS

In this work, a modified citrate–sulfate (Carey Lea) method has been used to synthesize hydrosols of silver metal nanoparticles with a median particle size of 8.4 nm and a concentration of 30 g/L stabilized with citrate ions and products of their partial decomposition. The obtained hydrosols have been used to study the features of the transfer of silver NPs into the phase of *o*-xylene in the presence of cetyltrimethylammonium bromide and ethanol. Using XPS, IR spectroscopy, and thermal analysis, it has been found that, during the extraction process, cetyltrimethylammonium cations replace sodium cations in the adsorption layer on the surface of silver nanoparticles, thereby increasing their hydrophobicity and facilitating the transition into the phase of *o*-xylene (extraction degree of 62.5%). At the same time, the size and morphology of the nanoparticles remain actually unchanged. The resulting silver organosols are stable in the course of

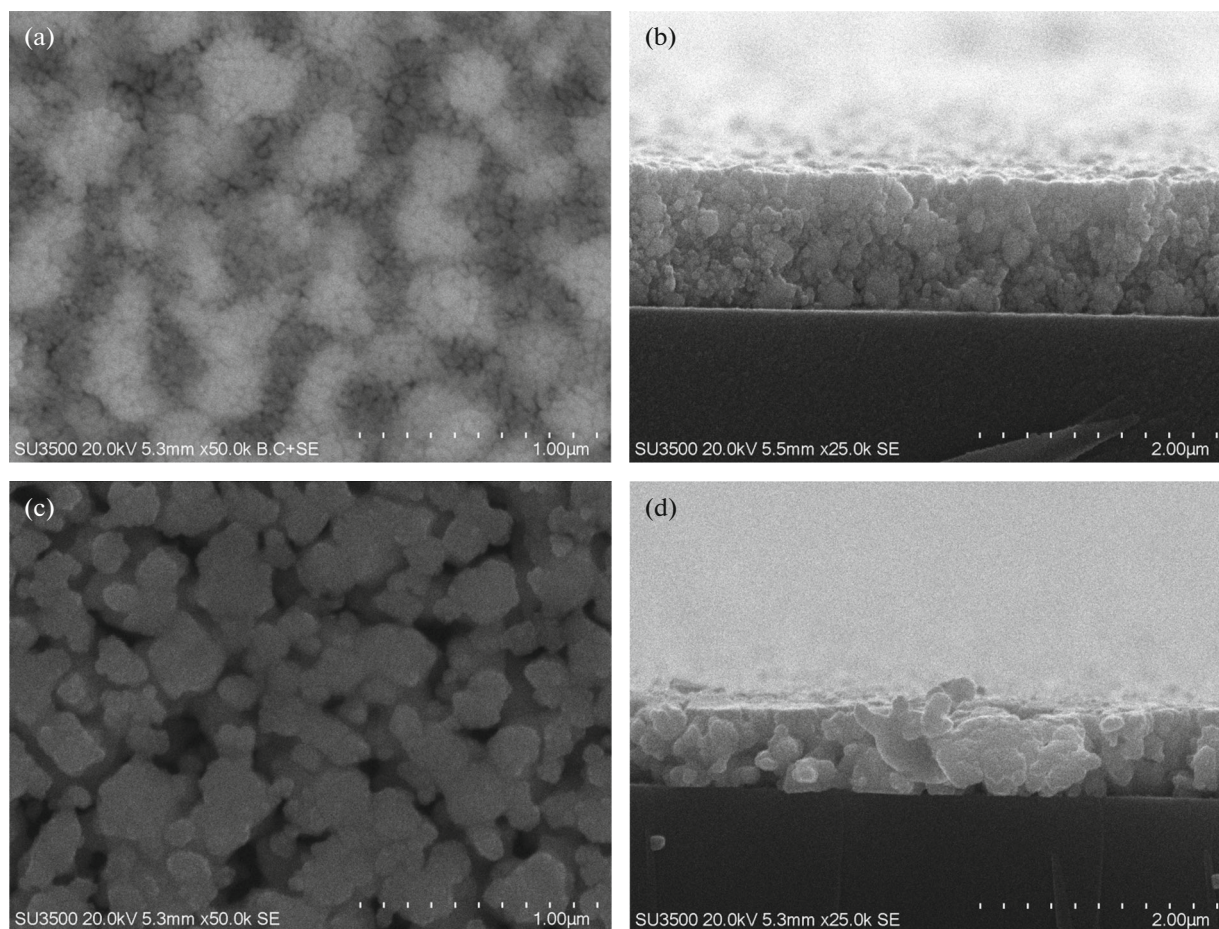


Fig. 7. SEM micrographs of the (a, c) surface and (b, d) cross section of films (a, b) before and (c, d) after annealing at 250°C.

four successive cycles of drying and redispersing in *o*-xylene and can be concentrated by partial removal of the solvent to a metal content of 1800 g/L.

Before annealing, silver films obtained on the basis of the organosols have an electrical conductivity of about 68500 S/cm, which increases by more than

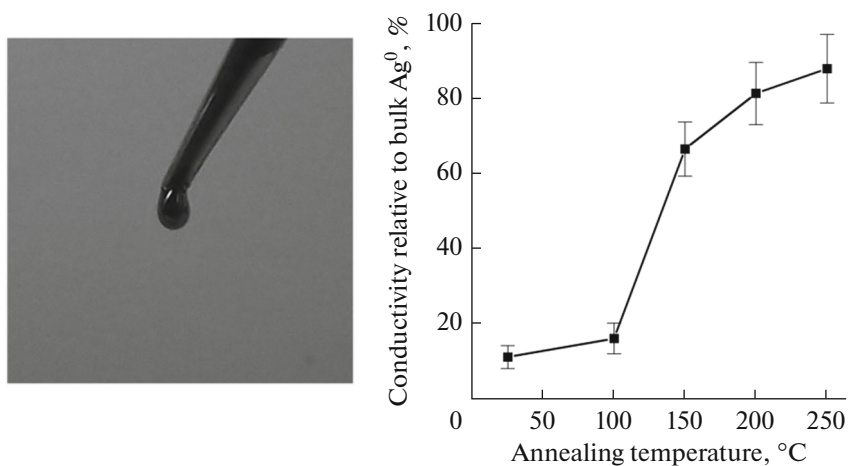


Fig. 8. Appearance of a droplet of organosol with a metal concentration of 1800 g/L and the dependence of the specific electrical conductivity of obtained films relative to bulk silver on annealing temperature.

6.0 and 7.4 times after heat treatment at 150 and 250°C, respectively.

FUNDING

The work was carried out with the financial support of the basic project FWES-2021-0014 of the Institute of Chemistry and Chemical Technology, Siberian Branch, Russian Academy of Sciences, and the Federal Program “Priority 2030” using the equipment of the Krasnoyarsk regional center for collective use of the Federal Research Center Krasnoyarsk Scientific Center, Siberian Branch, Russian Academy of Sciences.

CONFLICT OF INTEREST

The authors of this work declare that they have no conflicts of interest.

OPEN ACCESS

This article is licensed under a Creative Commons Attribution 4.0 International License, which permits use, sharing, adaptation, distribution and reproduction in any medium or format, as long as you give appropriate credit to the original author(s) and the source, provide a link to the Creative Commons license, and indicate if changes were made. The images or other third party material in this article are included in the article’s Creative Commons license, unless indicated otherwise in a credit line to the material. If material is not included in the article’s Creative Commons license and your intended use is not permitted by statutory regulation or exceeds the permitted use, you will need to obtain permission directly from the copyright holder. To view a copy of this license, visit <http://creativecommons.org/licenses/by/4.0/>

REFERENCES

1. Facibeni, A., *Silver Nanoparticles: Synthesis, Properties and Applications*, Dubai: Jenny Stanford Publishing, 2023. <https://doi.org/10.1201/9781003278955>
2. Prasher, P. and Sharma, M., *Silver Nanoparticles: Synthesis, Functionalization and Applications*, Singapore: Bentham Science Publishers, 2022. <https://doi.org/10.2174/97898150505301220101>
3. Nastulyavichus, A.A., Kudryashov, S.I., Emelyanenko, A.M., and Boinovich, L.B., Laser generation of colloidal nanoparticles in liquids: Key processes of laser dispersion and main characteristics of nanoparticles, *Colloid J.*, 2023, vol. 85, no. 2, pp. 233–250. <https://doi.org/10.1134/S1061933X23600136>
4. Borovikova, S.A., Shafikulina, A.D., Revina, A.A., and Buryak, A.K., The use of size-exclusion chromatography and laser desorption/ionization for studying silver nanoparticles synthesized in reverse micelles, *Colloid J.*, 2022, vol. 84, no. 6, pp. 663–671. <https://doi.org/10.1134/S1061933X22700119>
5. Uryupina, O.Ya., Urodkova, E.K., Tikhonov, V.E., Zhavoronok, E.S., and Senchikhin, I.N., Formation of silver nanoparticles in aqueous oligochitosan solutions, *Colloid J.*, 2021, vol. 83, no. 1, pp. 142–150. <https://doi.org/10.1134/S1061933X21010142>
6. Vysotskii, V.V., Uryupina, O.Ya., Urodkova, E.K., Zaitseva, A.V., and Tikhonov, V.E., Effect of reductant (chitosan) molecular mass on the synthesis of silver nanoparticle dispersions and the properties of ring deposits resulting from evaporation of droplets of these dispersions, *Colloid J.*, 2020, vol. 82, no. 6, pp. 641–648. <https://doi.org/10.1134/s1061933x20060204>
7. Vorobyev, S.A., Novikova, G.V., Demina, A.V., Shidlovskiy, I.P., and Volochaev, M.N., Synthesis and synergistic effect of antibacterial composites based on concentrated hydrosols of silver nanoparticles combined with cephalosporins antibiotics, *Inorg. Chem. Commun.*, 2022, vol. 144, no. 1, p. 109862. <https://doi.org/10.1016/j.inoche.2022.109862>
8. Yang, J., Lee, J.Y., and Ying, J.Y., Phase transfer and its applications in nanotechnology, *Chem. Soc. Rev.*, 2011, vol. 40, no. 3, pp. 1672–1696. <https://doi.org/10.1039/B916790K>
9. Wei, W. and Gu, B., Preparation and characterization of silver nanoparticles at high concentrations, *ACS Symp. Ser.*, 2004, vol. 878, pp. 1–14. <https://doi.org/10.1021/bk-2004-0878.ch001>
10. Sarathy, K.V., Raina, G., Yadav, R.T., Kulkarni, G.U., and Rao, C.N.R., Thiol-derivatized nanocrystalline arrays of gold, silver, and platinum, *J. Phys. Chem. B.*, 1997, vol. 101, no. 48, pp. 9876–9880. <https://doi.org/10.1021/jp971544z>
11. Sarkar, A., Kapoor, S., and Mukherjee, T., Oleic acid-assisted phase transfer of nanosized silver colloids, *Res. Chem. Intermed.*, 2010, vol. 36, pp. 403–410. <https://doi.org/10.1007/s11164-010-0150-5>
12. Wang, X. and Chen, Y., A new two-phase system for the preparation of nearly monodisperse silver nanoparticles, *Mater. Lett.*, 2008, vol. 62, no. 28, pp. 4366–4368. <https://doi.org/10.1016/j.matlet.2008.07.034>
13. Nath, S., Ghosh, S.K., Praharaaj, S., Panigrahi, S., Basu, S., and Pal, T., Silver organosol: Synthesis, characterisation and localised surface plasmon resonance study, *New J. Chem.*, 2005, vol. 29, no. 12, pp. 1527–1534. <https://doi.org/10.1039/B508730A>
14. Cho, S.T., US Patent 8,591,624 B2, Microneedles for minimally invasive drug delivery, 2013.
15. Kubo, H., Ohshima, Y., Nakamura, N., Noguchi, H., Taniuchi, J., Makita, Y., US Patent 2017/0215279 A1, Nano-sized silver particle ink, nano-sized silver particle sintered body, and method for producing nano-sized silver particle ink, 2017.
16. Lea, M.C., Allotropic forms of silver, *Amer. J. Sci.*, 1889, vol. 3, no. 222, pp. 476–491. <https://doi.org/10.2475/ajs.s3-37.222.476>
17. Vorobyev, S.A., Likhatski, M.N., Romanchenko, A.S., Fetisova, O.Y., Kazachenko, A.S., Volochaev, M.N., and Mikhlin, Y.L., Fabrication of extremely concentrated silver hydrosols without additional stabilizers, *ACS Sustainable Chem. Eng.*, 2020, vol. 8, no. 46,

- pp. 17225–17233.
<https://doi.org/10.1021/acssuschemeng.0c06006>
18. Vorobyev, S.A., Likhatski, M.N., Romanchenko, A.S., Ivanenko, T.Y., Masharova, D.A., Volochaev, M.N., and Mikhlin, Y.L., The influence of the reaction conditions on the size of silver nanoparticles in Carey Lea's concentrated sols, *J. Sib. Fed. Univ., Chem.*, 2020, vol. 13, no. 3, pp. 372–384.
<https://doi.org/10.17516/1998-2836-0190>
 19. Vorobyev, S., Vishnyakova, E., Likhatski, M., Romanchenko, A., Nemtsev, I., and Mikhlin, Yu., Reactivity and chemical sintering of Carey Lea silver nanoparticles, *Nanomaterials*, 2019, vol. 9, no. 11, p. 1525.
<https://doi.org/10.3390/nano9111525>
 20. Mikhlin, Y., Vorobyev, S., Saikova, S., Vishnyakova, E., Romanchenko, A., Zharkov, S., and Larichev, Yu., On the nature of citrate-derived surface species on Ag nanoparticles: Insights from X-ray photoelectron spectroscopy, *Appl. Surf. Sci.*, 2018, vol. 427 (B), pp. 687–694.
<https://doi.org/10.1016/j.apsusc.2017.09.026>
 21. Krebs, F.C., Fabrication and processing of polymer solar cells: A review of printing and coating techniques, *Sol. Energy Mater. Sol. Cells*, 2009, vol. 93, no. 4, pp. 394–412.
<https://doi.org/10.1016/j.solmat.2008.10.004>
 22. Vishnyakova, E.A., Saikova, S.V., Nikolaeva, R.B., and Mikhlin, Y.L., Synthesis of anisotropic silver nanoparticles and investigation of their sensory properties, *Russ. J. Inorg. Chem.*, 2012, vol. 57, no. 2, pp. 152–159.
<https://doi.org/10.1134/S0036023612020283>
 23. Irzhak, T.F. and Irzhak, V.I., On the digestive ripening mechanism, *Russ. J. Phys. Chem. A*, 2020, vol. 94, pp. 1439–1442.
<https://doi.org/10.1134/S0036024420070146>
 24. Bichara, L.C., Lanús, H.E., Ferrer, E.G., Gramajo, M.B., and Brandan, S.A., Vibrational study and force field of the citric acid dimer based on the SQM methodology, *Adv. Phys. Chem.*, 2011, vol. 2011, no. 1, p. 347072.
<https://doi.org/10.1155/2011/347072>
 25. Mikhlin, Y.L., Vishnyakova, E.A., Romanchenko, A.S., Saikova, S.V., Likhatski, M.N., Larichev, Y.V., Tuzikov, F.V., Zaikovskii, V.I., and Zharkov, S.M., Oxidation of Ag nanoparticles in aqueous media: Effect of particle size and capping, *Appl. Surf. Sci.*, 2014, vol. 297, pp. 75–83.
<https://doi.org/10.1016/j.apsusc.2014.01.081>
 26. Fang, J., Zhao, H., Liu, Q., Zhang, W., Gu, J., Su, Y., Abbas, W., Su, H., You, Z., and Zhang, D., AgBr/diatomite for the efficient visible-light-driven photocatalytic degradation of Rhodamine B, *J. Nanopart. Res.*, 2018, vol. 20, p. 61.
<https://doi.org/10.1007/s11051-018-4151-4>
 27. Park, J.W. and Shumaker-Parry, J.S., Structural study of citrate layers on gold nanoparticles: Role of intermolecular interactions in stabilizing nanoparticles, *J. Am. Chem. Soc.*, 2014, vol. 136, no. 5, pp. 1907–1921.
<https://doi.org/10.1021/ja4097384>
 28. Mazov, I., Kuznetsov, V.L., Simonova, I.A., Stadnichenko, A.I., Ishchenko, A.V., Romanenko, A.I., Tkachev, E.N., and Anikeeva, O.B., Oxidation behavior of multiwall carbon nanotubes with different diameters and morphology, *Appl. Surf. Sci.*, 2012, vol. 258, no. 17, pp. 6272–6280.
<https://doi.org/10.1016/j.apsusc.2012.03.021>
 29. Okpalugo, T.I.T., Papakonstantinou, P., Murphy, H., McLaughlin, J., and Brown, N.M.D., High resolution XPS characterization of chemical functionalised MWCNTs and SWCNTs, *Carbon*, 2005, vol. 43, no. 1, pp. 153–161.
<https://doi.org/10.1016/j.carbon.2004.08.033>
 30. Cheng, Z., Tang, S.W., Feng, J., and Wu, Y., Biosynthesis and antibacterial activity of silver nanoparticles using *Flos Sophorae Immaturus* extract, *Heliyon*, 2022, vol. 8, no. 8, p. e10010.
<https://doi.org/10.1016/j.heliyon.2022.e10010>
 31. Pyatnitskii, I.V. and Sukhan, V.V., *Analiticheskaya khimiya srebra* (Analytical Chemistry of Silver), Moscow: Nauka, 1975.
 32. Poleeva, E.V., Arymbaeva, A.T., Bulavchenko, O.A., Plyusnin, P.E., Demidova, M.G., and Bulavchenko, A.I., Preparation of conductive silver films from electrophoretic concentrates stabilized with sorbitan monooleate and sodium bis(2-ethylhexyl)sulfosuccinate in n-Decane, *Colloid J.*, 2020, vol. 82, no. 3, pp. 295–302.
<https://doi.org/10.1134/S1061933X20030072>
 33. Popovetskiy, P.S., Arymbaeva, A.T., Bordzilovskiy, D.S., Mayorov, A.P., Maksimovski, E.A., and Bulavchenko, A.I., Synthesis and electrophoretic concentration of silver nanoparticles in water-in-oil emulsions of sodium bis(2-ethylhexyl) sulfosuccinate and preparation of conductive from them coatings by selective laser sintering, *Colloid J.*, 2019, vol. 81, no. 4, pp. 439–445.
<https://doi.org/10.1134/S1061933X19040112>

Publisher's Note. Pleiades Publishing remains neutral with regard to jurisdictional claims in published maps and institutional affiliations.